Zero-Current-Switched Three-Phase SVM-Controlled Buck Rectifier

Esteban Sanchis, *Member, IEEE*, Enrique Maset, *Member, IEEE*, Jose A. Carrasco, Juan B. Ejea, Agustin Ferreres, Enrique Dede, *Member, IEEE*, Vicente Esteve, *Member, IEEE*, José Jordan, and Rafael Garcia-Gil

***Abstract*—A zero-current-transition (ZCT) cell is analyzed and designed to be used with a three-phase pulsewidth-modulation buck rectifier. This rectifier was space-vector controlled and used unidirectional current switches. The proposed ZCT circuit is load independent and achieves a high noise and voltage stress reduction and provides ZCTs to almost all transitions of the rectifier's switches and to the additional auxiliary switches. Theoretical equations have been obtained for design purposes. The circuit is easy to design and the driving signals for the auxiliary switches are also easy to obtain, as demonstrated in this paper.**

***Index Terms*—Power-factor correction, space-vector modulation (SVM), three-phase recitifier, zero-current switching (ZCS).**

I. Introduction

THE use of buck-type rectifiers in three-phase applications is necessary if we need an output voltage lower than 2.12 V_{RMS} of the phase voltage. If the output voltage should be higher than 2.45 V_{RMS} a boost-type topology would be chosen.

Previous studies of zero-current-transition (ZCT) circuits present applications for three-phase boost-type rectifiers [1], but not for buck rectifiers and, in this paper, we analyze and design a new ZCT circuit [6] suitable for buck-type rectifiers which will highly improve its electromagnetic interference (EMI) emissions and greatly reduce voltage stress of the main switches. Some induction heating applications will require the use of a step-down rectifier when the use of a parallel resonant load means a current-fed inverter and where the power is controlled by changing the voltage to the filter inductor (current source). In this case, if we use a buck rectifier we could achieve current-source behavior, if a current loop is added to the rectifier, and power-factor correction is also provided. Other alternative solutions have been presented in [7] and [8] for telecom applications.

II. Space-Vector Modulation (SVM) Applied to Three-Phase Buck Rectifiers

SVM theory was first developed for electrical machines but in the last few years, thanks to the great advances in microprocessor technology, it has also been widely applied to rectifier and inverter control. Two great advantages of SVM are reduced harmonic content and a higher modulation index than other modulation techniques [9]. Additional benefits are that mean input current is naturally in phase with input voltage and that active displacement factor correction is possible [10]. This kind of modulation technique assures that the power factor is 1. Although the input current is switched, with the appropriate input filter it becomes purely sinusoidal. The delay introduced by the filter can be compensated by SVM and input current will be in phase with input voltage. The only content of harmonic distortion is at switching frequency, which normally is much higher than the line frequency (normally around 500 times higher). Therefore, international harmonic norms will be satisfied. These advantages are achievable with the use of fast enough microprocessors or digital signal processors (DSPs) which could perform the complex calculation to obtain the right duty cycle of each switch.

Its basic idea is that each switch combination (either ON or OFF) of the whole rectifier represents a vector (current vector in the case of a buck rectifier and voltage vector in the case of a boost rectifier) which can be used to generate any desired input current as seen in Fig. 1. If we assume that the load current of the rectifier shown in Fig. 2 (please do not take into account the

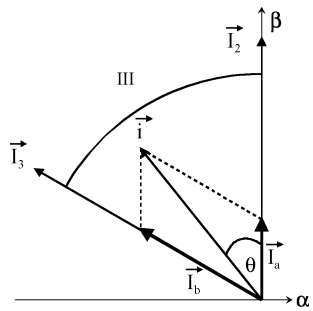

Fig. 1. Space-vector generation with two base space vectors in a buck rectifier. The radius of the circumference is equal to I_0 and represents the load current.

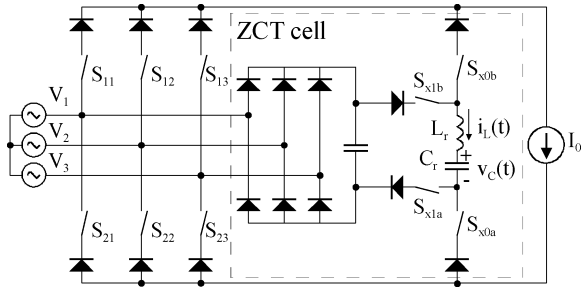

Fig. 2. Buck rectifier with ZCT circuit.

Manuscript received October 24, 2003; revised January 28, 2004. Abstract published on the Internet March 14, 2005.

E. Sanchis, E. Maset, J. B. Ejea, A. Ferreres, E. Dede, V. Esteve, J. Jordan, and R. Garcia-Gil are with the Departamento de Ingeniería Electrónica/ETSE/Universitat de València, E-46100 Burjassot, Spain (e-mail: esteban.sanchis@uv.es).

J. A. Carrasco is with the Division Tecnología Electrónica/EPSE, Universitat de Miguel Hernández, E-03202 Elche, Spain (e-mail: jacarrasco@umh.es).

Digital Object Identifier 10.1109/TIE.2005.843968

ZCT cell) is constant and equal to I_0, then a switching law can be defined with (1) (1 = ON, 0 = OFF). This means that one switch of the upper switches must always be ON and one switch of the lower switches must be ON at the same time. This avoids a short of the input voltage sources and provides a path to the load current

$$S_{i1} + S_{i2} + S_{i3} = 1 \quad i \in \{1, 2\}. \tag{1}$$

As an example, we show in Fig. 1 how a current vector $\vec{i}$ is generated with two base space vectors ($\vec{I}_a = d_a\vec{I}_2$ and $\vec{I}_b = d_b\vec{I}_3$).

This translates into two duty cycles [d_a and d_b defined in (2) and (3)] applied to these two base space vectors. Each of these space vectors (there are a total of six possible and three null vectors) means a given switch configuration. In fact, I_2 is generated by the following switch configuration: $S_{11} = S_{13} = S_{21} = S_{22} = 0$ and $S_{12} = S_{23} = 1$. I_3 is generated by the switch configuration: $S_{11} = S_{13} = S_{22} = S_{23} = 0$ and $S_{12} = S_{21} = 1$

$$d_a = \frac{I_a}{I_0}\frac{\sqrt{3}}{2} = \frac{i\ \sin\left(\frac{\pi}{3} - \theta\right)}{I_0} \tag{2}$$

$$d_b = \frac{I_b}{I_0}\frac{\sqrt{3}}{2} = \frac{i\ \sin(\theta)}{I_0} \tag{3}$$

$$d_0 = 1 - d_a - d_b. \tag{4}$$

To fill up the whole period, the rest of the time, a null vector d_0 defined in (4) is applied which can be generated with one of the following switch combinations: $S_{11} = S_{21} = 1$, $S_{12} = S_{22} = 1$, or $S_{13} = S_{23} = 1$ (the rest of the switches are OFF in each configuration). This null vector corresponds to the freewheeling period of the buck rectifier.

III. Soft Switching in Three-Phase Rectifiers

The main difference between buck and boost topologies is the kind of switches that are used. Buck-type rectifiers need current unidirectional switches while boost-type rectifiers need current bidirectional switches. This means that we can use a normal transistor with its body diode in the case of a boost rectifier, but for the buck rectifier we need to connect a series diode with the transistor.

The series connection of diode and transistor is a major drawback for this topology if we want to apply a voltage soft-switching technique. As already mentioned in [2], we will have two parasitic capacitors connected in series, one of the diode and one of the transistor. Both capacitors vary with voltage and are of different values. If we want to implement a zero-voltage-switching (ZVS) scheme we need to connect large external capacitors to our devices and select their ratio in a way so as to achieve ZVS in the transistor. Although in [2] a ZVT scheme is proposed and simulated, all these problems are mentioned and this topology is discarded because of them.

If we still have to use this topology and want to decrease its switching stress we will have to find a new soft switching strategy. As the switch is unidirectional in current it seems more appropriated to choose a ZCS scheme. This is also a desirable solution in case that we have to use bipolar transistors like insulated gate bipolar transistors (IGBTs) or bipolar junction transistors (BJTs) because we will reduce their higher turn-off losses (current tail).

IV. Three-Phase Buck Rectifier With ZCT

The circuit we have looked for is a resonant tank which we would activate during all the transitions and which would carry all the inductor current (for simplicity, we will assume it to be a current source) during the resonance. At this point no current will be circulating through the corresponding branch which gives us the option of switching all required switches under zero current, which means lossless. An additional desirable feature of the circuit would be to also switch the auxiliary switches under zero current to overcome one of the most important drawbacks of ZCT circuits; ZCT circuits normally handle the full switch current, which means that we will not save any energy if we provide soft switching to the main switches but have to hard switch the auxiliary switches [3]. Load independence is also desirable to provide the main circuit with soft current transitions under all load conditions.

The circuit proposed which has all the previous mentioned features is shown in Fig. 2.

Although we need four auxiliary switches (S_{x0a}, S_{x0b}, S_{x1a}, S_{x1b}), the driving signal for S_{x0a} and S_{x0b} is the same. Switches S_{x1a} and S_{x1b} are also driven by the same signal. The use of two switches is necessary to isolate the tank of the rest of the circuit when it is recharged and on the other hand it is an advantage to have it because the voltage stress imposed by the resonant capacitor is shared by both switches, although not equally.

V. Principles of Operation

The different states of the circuit can be easily derived from Fig. 2 (the first 13 states are shown in Fig. 3) taking into account that the ZCT cell is activated (S_{x0}) during each commutation of the main switches. In between commutation of main switches, the ZCT cell is activated again (S_{x1}) to recharge the resonant tank. We show the calculated waveforms of the whole switching cycle in Fig. 4. We will assume that the rectifiers' switching frequency (30 kHz) is much higher than the line frequency (50 Hz) and, in our case, the applied control scheme is six-step SVM where the freewheeling period has been distributed in between both active states [4]. The working principle is very simple. We have a half period of resonance during each switching transition which provides us with a zero-current condition and a second half period resonance in between transitions to recharge the resonant capacitor C_r again to a positive voltage.

Due to the fact that the switches are unidirectional in current we can find three additional states ($[t_1 - t_{2a}]$, $[t_{5a} - t_6]$, and $[t_6 - t_{6a}]$) which have a variable duration and adjust the voltage at the resonant capacitor so that we always have the same kind of transition.

The proposed ZCT circuit is, thus, independent of the output current. On the other hand it provides zero-current switching (ZCS) to all transitions of the main switches and six of the eight transitions of the auxiliary switches during one-half period of the switching frequency.

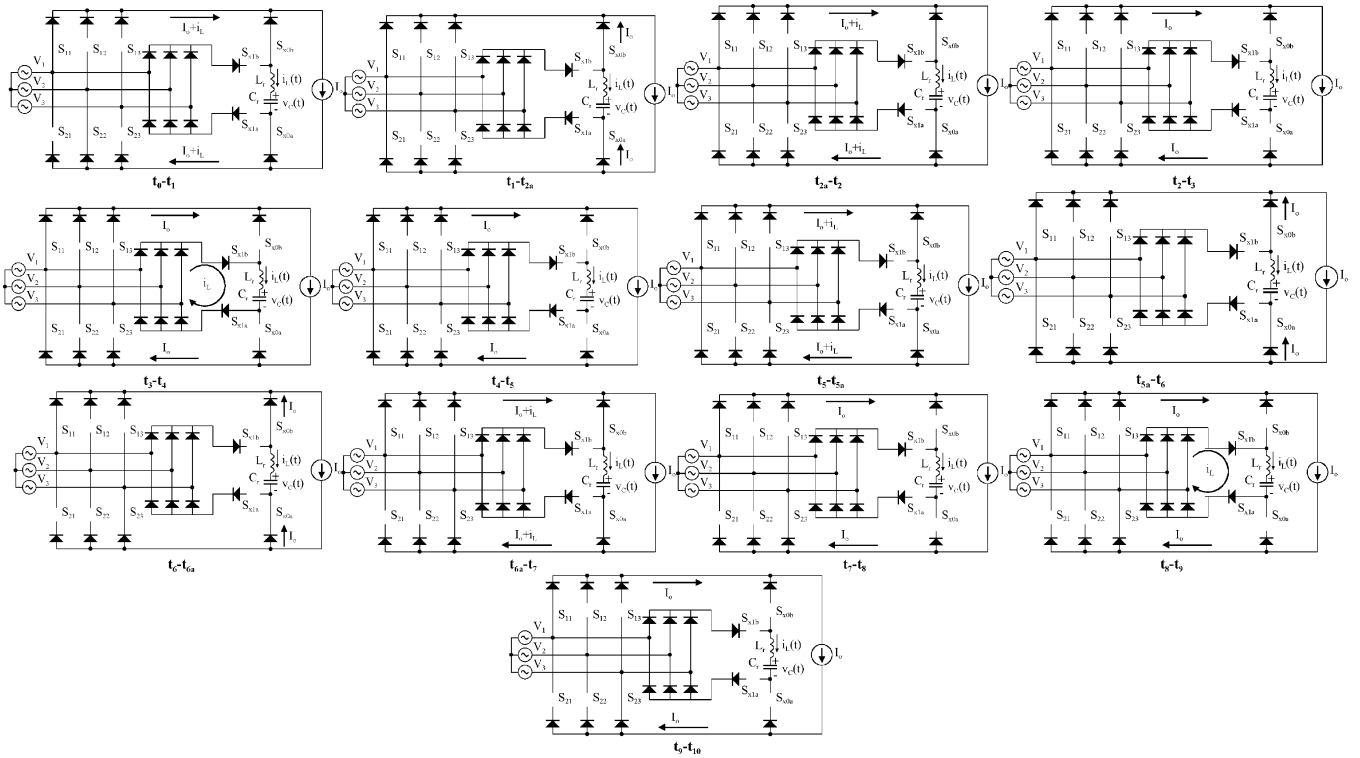

Fig. 3. First 13 states of the circuit.

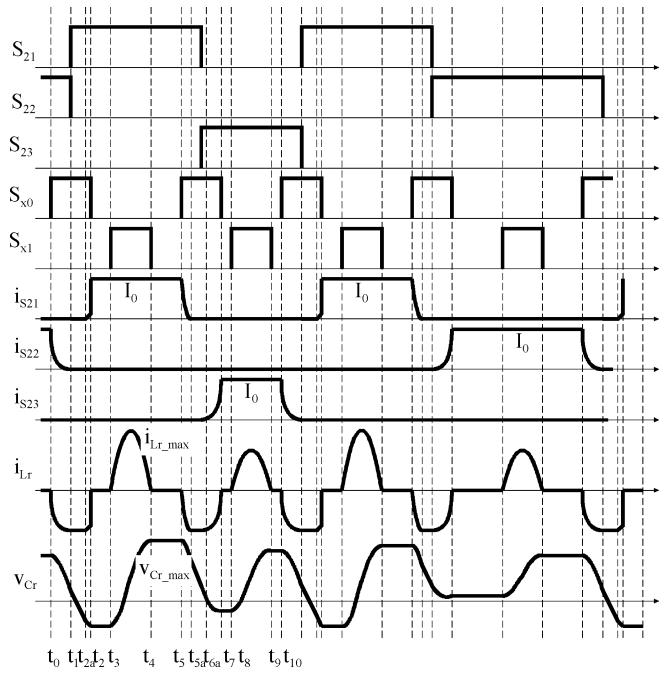

Fig. 4. Waveforms of the three-phase circuit at $\omega t = -15^\circ$ when $v_1 = 0.97\,V_{\rm pk}$, $v_2 = -0.71\,V_{\rm pk}$, and $v_3 = -0.26\,V_{\rm pk}$.

The transitions can be adjusted by changing the characteristic impedance of the resonant tank, assuming that we always have a fixed ON time ($t_{\rm on} = T_r/2$) of the auxiliary switches which activate the resonant tank. In fact, this is the only variable of our circuit we can change or adjust.

Let us explain all different timing intervals of the circuit to understand how it works. As the rectifiers' switching frequency

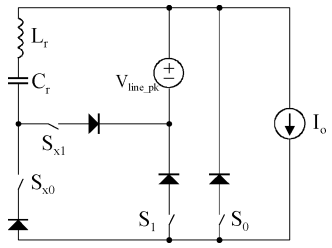

Fig. 5. Equivalent circuit of the buck rectifier with ZCT to study the proposed soft-switching technique.

(30 kHz) is much higher than the phase frequency (50 Hz in Europe), we can assume that the voltages do not change over a switching period.

To study the circuit we have simplified the system and have obtained the equivalent circuit shown in Fig. 5.

This circuit takes into account all the possible states. During the freewheeling state $[t_2$–$t_3]$, S_0 is ON and during the ON state $[t_7$–$t_8]$, S_1 is ON. The auxiliary switches S_{x1} and S_{x0} activate the resonant tank. We activate S_{x0} to achieve ZCT when we switch the main switches. When we switch S_{x1} ON we recharge the resonant capacitor, C_r. I_0 represents the output current and $V_{\rm line\_pk}$ is the voltage which is found in the three phase rectifier. In the real circuit $V_{\rm line\_pk}$ will have a 300-Hz ripple which changes its value between 1.5–1.7 times $V_{\rm pk}$ when it recharges the tank and between 0.9–1.7 times $V_{\rm pk}$ when it appears in the resonant mesh and it is providing ZCT to S_0 and S_1. This difference between the model and the real circuit will have little influence on the behavior of the real circuit compared to the model. It only affects the capacitor voltage and, therefore, the peak current of the resonance. The worst case is when we encounter a voltage source in the resonant path of the same value

as the one used to recharge the capacitor, because the capacitor must be charged to a much higher voltage than the voltage source in order to resonate in the "right direction." Thus, the model used represents the worst case of the real circuit.

The different states for half a switching period of the main switches are described. The intervals $[t_{5a}$–$t_6]$ and $[t_6$–$t_{6a}]$ have been merged into $[t_{5a}$–$t_{6a}]$ in the explanation which takes into account the real circuit and not the model. The model has only be used to obtain the different equations of each state.

A. t_0–t_1

Let us assume that we have just activated the auxiliary switch S_{x0} and S_{x1} is OFF. The resonance begins and current builds up through the tank until it reaches I_0. S_1 is ON and S_0 is OFF.

The equations of current through the resonant inductor i_L and voltage at the resonant capacitor v_C are

$$i_L(t) = \frac{V_{\text{line}} - V_C^-}{Z_r} \sin(\omega t) \tag{5}$$

$$v_C(t) = V_{\text{line}} - (V_{\text{line}} - V_C^-) \cos(\omega t) \tag{6}$$

where V_C^- is the voltage at the resonant capacitor at t_1.

The commutation of the main switches (S_1 = OFF, S_0 = ON) takes place at the midpoint of the interval $[t_0 - t_2]$. This is very close to t_1 but can also happen after t_1. In any case the current through the main switches is 0.

B. t_1–t_{2a}

The resonance will try to continue, but now without having a voltage source in its path, the current will, thus, try to increase but due to the series diode of S_0 current will be clamped to I_0 (S_1 = OFF, S_0 = ON, S_{x0} = ON, and S_{x1} = OFF). During this stage the resonant capacitor is, therefore, discharged with constant current (I_0).

C. t_{2a}–t_2

This will discharge the capacitor down to a voltage where the resonance will begin again with a current in the appropriated direction. This will reduce i_L, but the auxiliary switch S_{x0} will switch off before and this results in a hard-switching condition for the auxiliary switch. Now, still S_1 = OFF and S_0 = ON. The equations of this very short resonance are

$$i_L(t) = I_L^- \cos(\omega t) - \frac{V_C^-}{Z_r} \sin(\omega t) \tag{7}$$

$$v_C(t) = V_C^- \cos(\omega t) + I_L^- Z_r \sin(\omega t) \tag{8}$$

where V_C^- is the voltage at the resonant capacitor and I_L^- is the current through the resonant inductor at t_{2a}.

D. t_2–t_3

This is the normal operation interval of the circuit (S_1 = OFF, S_0 = ON, S_{x0} = OFF, and S_{x1} = OFF).

E. t_3–t_4

We force a resonance in the tank to recharge the resonant capacitor to the appropriated voltage to achieve ZCT in the following transition. To do this we have to add the line voltage to our resonant mesh. The main switches are S_1 = OFF and S_0 = ON and the auxiliary switches are S_{x0} = OFF and S_{x1} = ON. This interval takes a half period of the resonance and its equations are

$$i_L(t) = \frac{V_{\text{line}} - V_C^-}{Z_r} \sin(\omega t) \tag{9}$$

$$v_C(t) = V_{\text{line}} - (V_{\text{line}} - V_C^-) \cos(\omega t) \tag{10}$$

where V_C^- is the voltage at the resonant capacitor at t_3.

F. t_4–t_5

This is, again, a normal operation interval of the circuit (S_1 = OFF, S_0 = ON, S_{x0} = OFF, and S_{x1} = OFF).

G. t_5–t_{5a}

We again activate the resonant tank (S_{x0} = ON and S_{x1} = OFF) to force I_0 to circulate through it. In this case the resonance has a higher peak current due to the fact that the capacitor is charged to a high voltage and the resonant path does not include the line voltage. We reach I_0 much faster and due to the diode in series with S_0, the current is clamped to I_0, thus, zero-current condition is still achieved. Now, still S_1 = OFF and S_0 = ON. The equations of this, again, short resonant period are

$$i_L(t) = -\frac{V_C^-}{Z_r} \sin(\omega t) \tag{11}$$

$$v_C(t) = V_C^- \cos(\omega t) \tag{12}$$

where V_C^- is the voltage at the resonant capacitor at t_5.

H. t_{5a}–t_{6a}

C_r is discharged down to the line voltage with constant current I_0. At instant t_6 before it reaches this voltage the main switches are commutated under zero current (S_0 = OFF and S_1 = ON).

I. t_{6a}–t_7

Once we have reached the line voltage, resonance continues and, now, in the appropriate direction, thus reducing i_L almost to 0 A. The main switches are S_0 = OFF and S_1 = ON. Then, we switch off the auxiliary switch S_{x0} under almost zero current (we can consider it zero current). The resonant equations of this interval are

$$i_L(t) = I_L^- \cos(\omega t) + \frac{V_{\text{line}} - V_C^-}{Z_r} \sin(\omega t) \tag{13}$$

$$v_C(t) = V_{\text{line}} - (V_{\text{line}} - V_C^-) \cos(\omega t) + I_L^- Z_r \sin(\omega t) \tag{14}$$

where V_C^- is the voltage at the resonant capacitor and I_L^- is the current through the resonant inductor at t_{6a}.

J. t_7–t_8

We again have a normal operation interval (S_0 = OFF, S_1 = ON, S_{x0} = OFF, and S_{x1} = OFF).

K. t_8–t_9

During this half period of resonance we recharge C_r to a high voltage by activating S_{x1}. Notice that the auxiliary switches are also switched under zero current. The main switches are $S_0 =$ OFF and $S_1 =$ ON. This interval takes a half period of the resonance and its equations are

$$i_L(t) = \frac{V_{\text{line}} - V_C^-}{Z_r} \sin(\omega t) \tag{15}$$

$$v_C(t) = V_{\text{line}} - (V_{\text{line}} - V_C^-) \cos(\omega t) \tag{16}$$

where V_C^- is the voltage at the resonant capacitor at t_8.

L. t_9–t_{10}

This is the last normal operation interval of the first half period of the switching frequency. The main switches are still $S_0 =$ OFF and $S_1 =$ ON.

The study of the model which has the same different states as the real circuit shows that thanks to the diodes the current will be clamped to I_0 if the resonant current is larger than I_0. The result is that the circuit will be load independent and will achieve ZCT in almost all transitions. Only in the transition which happens during $[t_{2a} - t_2]$ are we hard switching the auxiliary devices (see Fig. 4).

To obtain useful design equations of the previous expressions it is necessary to calculate the resonant capacitor's maximum voltage. This is the most restrictive design consideration. To calculate this voltage we have to know the initial voltage and current conditions at the beginning of each interval. If this is done, taking into account that during some periods of time the capacitor is discharged at constant current, we obtain

$$V_{C_r\_\max} = 2V_{\text{line\_pk}} + I_0 Z_r \cos\left(\frac{V_{\text{line\_pk}}}{I_0 Z_r}\right). \tag{17}$$

This expression is obtained by knowing that the maximum voltage is sustained by the capacitor during $[t_4$- -$t_5]$ (see Fig. 4) and is, thus, the voltage $v_C(t_4)$. If we look at the expression for v_C at $[t3$- -$t4]$ we see that

$$V_{C_r\_\max} = 2V_{\text{line\_pk}} - v_C(t_2). \tag{18}$$

We can assume as a good approximation, taking into account that the resonance is very short and hard switching takes place at t_2, that $v_C(t_2)$ is

$$v_C(t_2) = -I_0 Z_r \sin(\omega t_2) \tag{19}$$

and as t_2 is

$$t_2 = \frac{\pi}{2\omega} - V_{\text{line}} \frac{C_r}{I_0} \tag{20}$$

so (17) is obtained.

All these expressions do not take losses into account. Losses play an important role and lower the voltage values and current values but are very difficult to evaluate because they depend mainly on parasitic elements of the circuit.

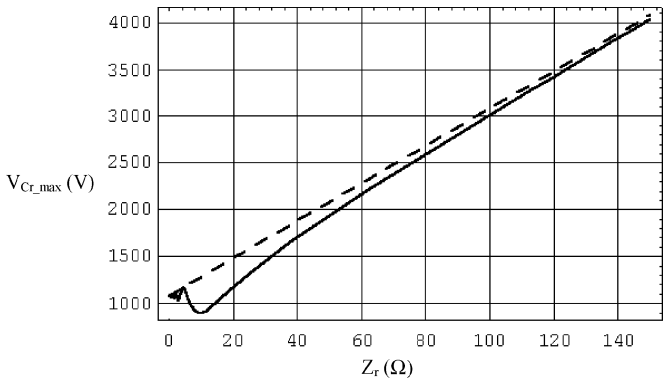

Fig. 6. Graphical representation of the expression of $V_{Cr\_\max}$ (bold line) and its approximation, where $\cos(V_{\text{line\_pk}}/I_0 Z_r) = 1$ (dashed line). $V_{\text{line\_pk}} = 540$ V, $I_0 = 20$ A.

VI. Design Procedure

The design procedure is straightforward. First, we have to fix the maximum voltage we want to have on the resonant capacitor, which is the main restriction of the circuit. Then, we need to know the duration of the resonant period which depends on how many ZCTs we want to have. We are not losing duty cycle with this technique because I_0 keeps on flowing and the output voltage is still applied to the output inductor independently of the ZCT circuit. The only limitation is that we have to recharge the capacitor after each resonance which means that we need a time gap between each ZCT. If two transitions are too close together (very small duty cycles d_a and d_b), we will not be able to apply ZCT to both. These considerations help us to fix the resonant frequency. As the ZCT circuit is load independent, we only have to fix the characteristic impedance of the resonant tank for the full load of the system.

The equation of maximum voltage at the resonant capacitor does not have an algebraic solution and we will have to make an approximation or solve it numerically. A possible approximation is to suppose that $\cos(V_{\text{line\_pk}}/I_0 Z_r) = 1$. The graphical representation of both equations is shown in Fig. 6. The dashed line is the approximation and the bold line is the equation including the cosinus. We can see that the error is small.

For the design we will use the approximation, which results in a higher capacitor voltage. In this case, we can solve for Z_r

$$Z_r = \sqrt{\frac{L_r}{C_r}} = \frac{V_{C_r\_\max} - 2V_{\text{line\_pk}}}{I_0} \tag{21}$$

$$T_r = 2\pi\sqrt{L_r C_r}. \tag{22}$$

With these two equations, fixing T_r and $V_{Cr\_\max}$ and knowing $V_{\text{line\_}pk}$ and I_0, we can already determine L_r and C_r. $V_{\text{line\_}pk}$ is the line voltage and I_0 is the maximum current which has to circulate through our main switches.

On the other hand, it has to be noted that if we consider losses in our circuit, which happens in real circuits, maximum voltage at the capacitor is lower at steady state. Fig. 5 shows the ideal circuit model without losses. From this point of view, losses will help us to maintain a reasonable capacitor voltage and, thus, an acceptable voltage stress at our auxiliary switches.

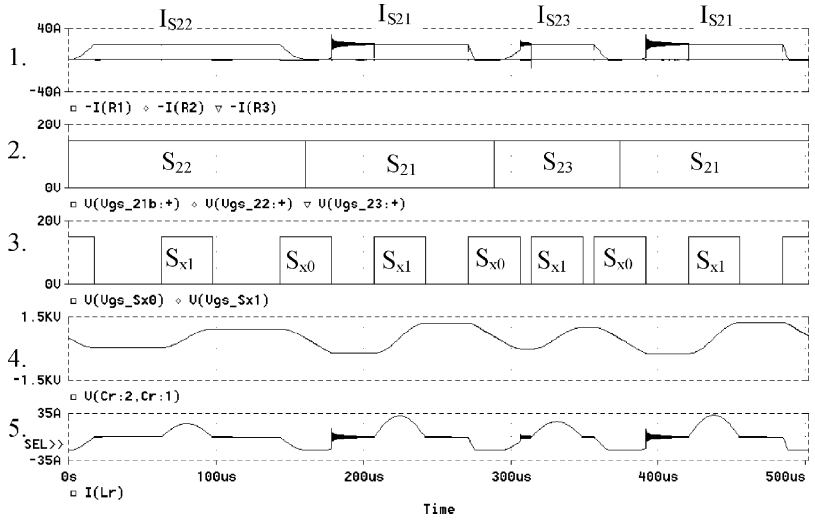

Fig. 7. Plots from top to bottom are 1: current through switches $S_{21}(-I(R1))$, $S_{22}(-I(R2))$, and $S_{23}(-I(R3))$; 2: drive signals of the mains switches; 3: drive signals of the auxiliary switches; 4: voltage of the resonant capacitor; 5: current through the resonant tank.

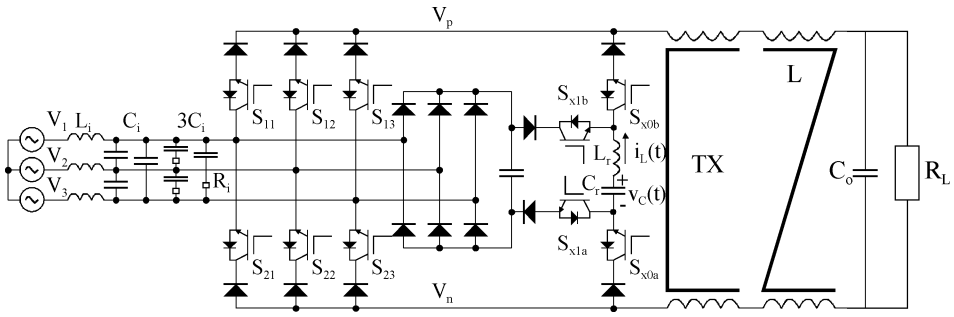

Fig. 8. Circuit diagram. Component list: diodes: HFA32PA120C; main switches: MG50Q2YS40; auxiliary switches: IRGPH50KD2; TX: common-mode filter; L: coupled filter inductor $L = 940\ \mu$H; output capacitor: $C_o = 5$ mF; input filter: $C_i = 2\ \mu$F; $L_i = 750\ \mu$H; $R_i = 25\ \Omega$.

Simulation of the circuit demonstrates its operation principle and validates the model and its timing analysis. In Fig. 7, we can see the simulation results of the three phase circuit, where the resonant period has been greatly enlarged compared to the switching period to enhance the ZCTs. The high-frequency ringing in the current waveforms of Fig. 7, plot 5, shows us when a hard switching occurs. We observe that there are only two really hard-switching instants for the auxiliary switches.

VII. Experimental Results

A 1-kW experimental prototype has been built. It is a three-phase space-vector-controlled rectifier which has the ZCT scheme added as shown in Fig. 2. The unit has been tested under its worst case which happens during maximum output current. Its specifications are as follows:

$$V_{\text{line}} = 380\ \text{V}_{\text{RMS}}$$
$$V_0 = 50\ \text{V}$$
$$f_{\text{sw}} = 30\ \text{kHz}$$
$$I_0 = 20\ \text{A}.$$

Fig. 8 shows the schematic diagram.

The circuit is controlled by an analog/digital control which uses a DSP to distribute the space-vector-modulated duty cycles with a six-step pattern as in [4] and the feedback is done with classical operational amplifiers which give us the option to include a current loop ("conductance control" [5]) which has been successfully implemented.

The ZCT cell switches' driving signals are generated from additional auxiliary signals generated by the DSP to drive the main switches and these signals will trigger a few monostable circuits to generate the drive signals for the ZCT cell.

To design the ZCT circuit we have used the approximated equation (21) obtained earlier in the paper. With the specifications and fixing $T_r = 2\ \mu$s and $V_{C\max} = 1500$ V we obtain

$$Z_r = \sqrt{\frac{L_r}{C_r}} = \frac{V_{C_r\_\max} - 2V_{\text{line\_pk}}}{I_0} = 21\ \Omega \qquad (23)$$

and taking into account the losses we choose Z_r a little bit larger. In fact, as Z_r is the only variable that we can change, once we have fixed the resonant period, we will have to adjust it experimentally if the resonant maximum current does not reach the full-load current. This would mean that we would not reach zero current under full load and lose the zero-current condition at a lower load. The circuit adjusts itself to the load current and will present lower resonant currents at lower load levels [see that the maximum resonant capacitor voltage depends on the load current, (17)].

We choose

$$Z_r = 25\ \Omega$$

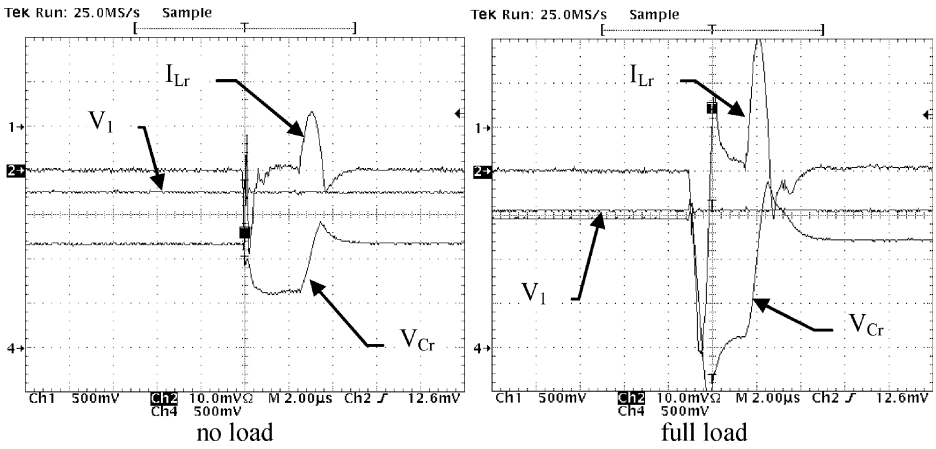

Fig. 9. Waveforms of the resonant tank of the ZCT cell. Ch1: $0.04 * V_{\text{phase1}}$ (5 V/div); Ch2: I_{Lr} (5 A/div); Ch4: V_{Cr} (250 V/div). $V_{\text{line}} = 380\,\text{V}_{\text{RMS}}$; $V_0 = 50$ V.

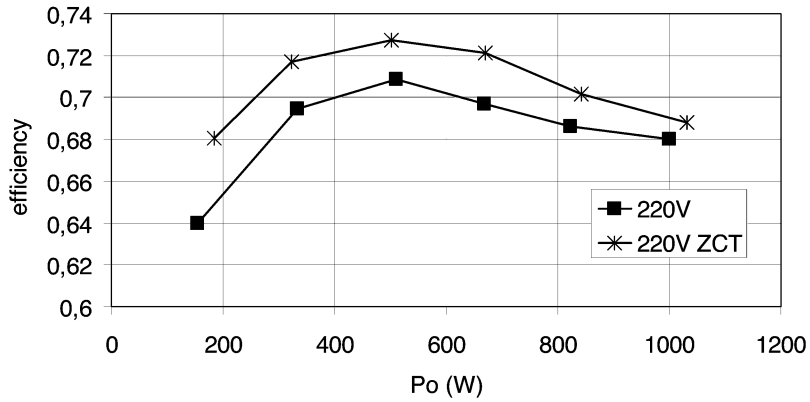

Fig. 10. Efficiency of the buck-type rectifier with and without ZCT circuit for nominal input phase voltage. The losses of the ZCT circuit are not considered.

and

$$C_r = \frac{T_r}{2\pi Z_r} = 12.7\ \text{nF}. \tag{24}$$

We have chosen to put two capacitors in parallel (10 nF + 2.2 nF) to increase its current capabilities

$$C_r = 12.2\ \text{nF}$$

and L_r is

$$L_r = \frac{{T_r}^2}{4\pi^2 C_r} = 8.3\ \mu\text{H}. \tag{25}$$

The ZCT circuit has been built with high-voltage IGBTs which are switched at very high frequency ($T_r = 2\ \mu\text{s} \Leftrightarrow f_r = 500$ kHz). The use of MOS devices would be more adequate to be able to switch easily at this high frequency (500 kHz).

We show the resonant tank waveforms where we have delayed the charging half period from the discharging half period to improve efficiency of the whole tank. It can be clearly seen that the current waveforms are not clamped at 0 A once the switch is OFF due to reverse recovery of the diodes. The voltage waveforms are also very similar to the simulated one, although of lower value due to losses. It has to be taken into account that the resonance frequency chosen was off 500 kHz and the simulation had a resonant frequency of 10 kHz. This had the drawback in the simulation that the ZCT cell only was useful in a few transitions of the main switches, because as soon as the duty cycle became small no recharging time was available and the operation of the ZCT was inhibited.

It was very difficult to acquire the right waveforms due to triggering problems. Triggering with the line voltage was tried, but at this time scale no stability of the signal was achieved.

Under no-load conditions C_r was charged at a lower voltage as expected and once the ZCT cell was activated the charge of C_r remained positive. However, under full load C_r was charged at a much higher voltage and when the ZCT cell was activated V_{Cr} reached 0 V (Fig. 9).

The efficiency of the rectifier itself has been increased more than two points as shown in Fig. 10 although it is still kept below 75%. There are several reasons for this low efficiency. First of all, the buck rectifier topology itself has very large conduction losses because the current always flows through two switches and two diodes in series. With our selected components this was a loss of 20% of power (2.5-V voltage loss in diode and 2.5-V voltage loss in IGBT with 20 A at 1-kW output power). If inductor losses, input filter losses, current sense resistor losses, and other losses are added we will easily reach 73% efficiency. All switches were also provided with an *RC* snubber to avoid excessive heating of the semiconductor devices. This also lowered the efficiency, especially that of the auxiliary switches of

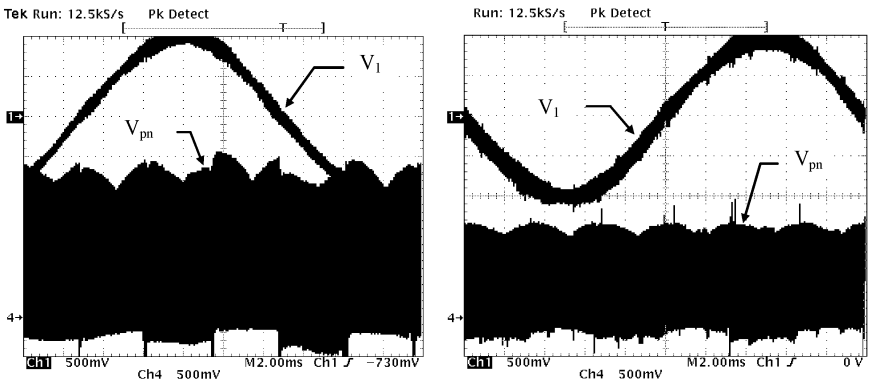

a: without ZCT b: with ZCT

Fig. 11. Noise figures of the rectifier with and without ZCT circuit measured at V_{pn}. Ch1: $0.04 * V_{\text{phase1}}$ (5 V/div); Ch4: V_{pn} (250 V/div). $V_{\text{line}} = 380\,\text{V}_{\text{RMS}}$; $V_0 = 50$ V; $I_0 = 20$ A; $L_r = 8.5\ \mu$H; $C_r = 12.2$ nF.

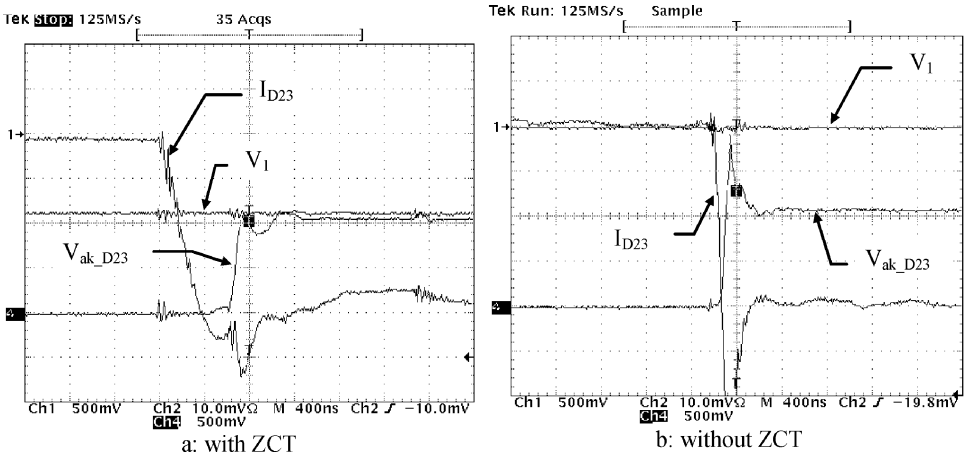

a: with ZCT b: without ZCT

Fig. 12. Transitions with and without ZCT circuit. Ch1: $0.04 * V_1$ (5 V/div); Ch2: I_{D23} (5 A/div); Ch4: V_{ak_D23} (250 V/div). $V_{\text{line}} = 380\,\text{V}_{\text{RMS}}$; $V_0 = 50$ V; $I_0 = 20$ A; $L_r = 8.5\ \mu$H; $C_r = 12.2$ nF.

the ZCT cell which worked at 500 kHz. To improve this efficiency we suggest several solutions. A diode can be placed as a freewheeling diode and during the dead time the current will not flow anymore through a leg of the rectifier. The component selection could be improved with state-of-the art components to reduce conduction and switching losses. The current sense resistor could be replaced by a Hall-effect sensor. Note, also, that a design with a larger output voltage would have lower output current and, therefore, fewer losses.

On the other hand its voltage stress is greatly reduced as shown in Fig. 11.

Although the circuit is load independent, the high-voltage diodes used (IR HFA32PA120C, $t_{rr} = 30$ ns) still present a small reverse-recovery current (3 A) under the slow di/dt provided by the resonance as predicted by the manufacturer. This means that the diodes do not clamp the current through the main switches to 0 A and we will switch our main switches at our reverse-recovery current (about -3 A) for loads smaller than the full load, as shown in Fig. 12.

The main benefit obtained from the circuit is the noise reduction and, therefore, the voltage stress reduction in the main switches (Fig. 11). This confirms that the switching is done under zero current during almost all transitions and this, of course, reduces the losses of the main switches which is confirmed by the increase of efficiency (Fig. 10). The spikes we see in Fig. 11(b) show that ZCT commutation is lost when small duty cycles appear and no recharging time is available. Then, the DSP inhibits the ZCT.

Fig. 12(b) shows how a large reverse-recovery current occurs when the ZCT circuit is not applied. This also results in a large voltage spike (about 500 V).

For optimal operation the time between the soft-switching half period and the recharging half period (as was done in the simulation) has been increased. This reduced the losses in S_{x0}.

VIII. Conclusion

A new ZCT circuit has been analyzed and designed which provides soft switching not only to the main switches for all its transitions but also to the auxiliary switches during at least six transitions of eight during one half period of the main switching frequency. One of these two transitions which is not done under zero current is done under almost zero current and the other one is done under a smaller current than full current. The operation and design of the ZCT circuit is very simple. Approximate mathematical formulas of the circuit show that the capacitor voltage is very high and depends on Z_r, I_0, and the line voltage, although the real circuit shows that voltage stress in the

resonant capacitor is reduced due to resistive losses in the resonant circuit. This fact reduces the voltage stress in the auxiliary switches. The circuit operation is also load independent.

The circuit provides us with soft switching for three-phase buck-type rectifiers. Voltage stress and, therefore, EMI is greatly reduced in the main switches as demonstrated experimentally. Efficiency in the rectifier is greatly improved although overall efficiency is not as high as expected due to the switching losses in the IGBT of the ZCT circuit. A MOSFET should be used instead.

REFERENCES

[1] G. Hua, E. X. Yang, Y. Jiang, and F. C. Lee, "Novel zero-current-transition PWM converters," in *Proc. IEEE PESC'93*, Jun. 1993, pp. 538–544.

[2] V. Vlatkovic, "Three-phase power conversion using soft-switching PWM techniques," Ph.D. dissertation, VPEC, Bradley Dept. Elect. Eng., Virginia Polytech. Inst. State Univ., Blacksburg, VA, 1994.

[3] H. Mao, F. C. Lee, X. Zhou, H. Dai, M. Cosan, and D. Boroyevic, "Improved zero-current-transition converters for high power applications," in *Proc. VPEC Seminar*, Sep. 1996, pp. 91–99.

[4] V. Vlatkovic and D. Boroyevic, "Digital-signal processor-based control of three-phase, space vector modulated converters," in *Proc. IEEE APEC'93*, 1993, pp. 888–894.

[5] D. O'Sullivan, H. Spruyt, and A. Crausaz, "PWM conductance control," in *Proc. IEEE PESC'88*, Apr. 1988, pp. 351–359.

[6] E. Sanchis-Kilders, E. Maset, J. A. Carrasco, and A. J. Dede, "Novel zero-current-transition circuit for three-phase buck rectifiers," in *Proc. IEEE PESC'97*, Jun. 1997, pp. 1260–1266.

[7] Y. Li, F. C. Lee, J. Lai, and D. Boroyevich, "A novel three-phase zero-current-transition and quasizero-voltage-transition (ZCT-QZVT) inverter/rectifier with reduced stress on devices and components," in *Proc. IEEE APEC'00*, Feb. 2000, pp. 1030–1036.

[8] C. Cuadros, S. Chandrasekaran, K. Wang, D. Boroyevich, and F. C. Lee, "Modeling, control and implementation of the quasi single stage three-phase zero-voltage zero-current switched buck rectifier," in *Proc. IEEE APEC'99*, Mar. 1999, pp. 248–254.

[9] H. W. van der Broeck, H. C. Skudelny, and G. V. Stanke, "Analysis and realization of a pulsewidth modulator based on voltage space vectors," *IEEE Trans. Ind Appl.*, vol. 24, no. 1, pp. 142–150, Jan./Feb. 1988.

[10] S. Hiti, V. Vlatkovic, D. Boroyevic, and F. C. Lee, "A new control algorithm for three-phase PWM buck rectifier with input filter displacement factor compensation," *IEEE Trans. Power Electron.*, vol. 9, no. 2, pp. 173–180, Mar. 1994.

Esteban Sanchis (M'00) was born in Valencia, Spain, in 1967. He received the M.Sc. degree in physics, with a specialization in electronics, and the Ph.D. degree from the Universitat de València, Burjassot, Spain, in 1990 and 1997, respectively.

From 1991 to 1992, he was with GH Electrotermia S.A. From 1992 to 1994 he was with the Power Conditioning Section of the European Space Agency, Noordwijk, The Netherlands. He then returned to the Universitat de València, where, from 1994 to 1999, he was an Assistant Professor and where, since 1999, he has been an Associate Professor and a member of the Laboratory of Industrial Electronics and Instrumentation (LEII). His main interests are industrial electronics and space power systems.

Enrique Maset (S'89–M'93) was born in Xàtiva, Spain, in 1965. He received the M.Sc. and Ph.D. degrees in physics from the Universitat de València, Burjassot, Spain, in 1988 and 1993, respectively.

He is currently an Associate Professor in the Electronic Engineering Department at the Universitat de València, where his main research areas include power-factor-correction techniques and high-frequency and soft-switching conversion techniques for industrial applications.

Jose A. Carrasco was born in Alicante, Spain, in 1967. He received the M.Sc. degree in physics and the Ph.D. degree from the Universitat de València, Burjassot, Spain, in 1990 and 1996, respectively.

He was with the European Space Agency in the European Space Research and Technology Center, Noordwijk, The Netherlands, for two years. In 1993, he joined the Laboratory of Industrial Electronics and Instrumentation (LEII) at the Universitat de València. In 1999, he joined the Universitat Miguel Hernàndez, Elche, Spain, where he is an Associate Professor. He has participated in several projects on power electronics and instrumentation for industrial and space applications and has produced nearly 100 technical papers in these fields. His main research areas include instrumentation, industrial networking, robust control techniques, and high-efficiency power conversion.

Juan B. Ejea was born in Xátiva, Spain, in 1969. He received the M.Sc. degree in physics, with a specialization in electronics, and the Ph.D.degree in electronics engineering from the Universitat de València, Burjassot, Spain, in 1993 and 2000, respectively.

His employment experience includes one year with GH Electrotermia S.A., two years with the Power Section of the European Laboratory for Particle Physics (CERN), Switzerland, and eight years as an Assistant Professor at the Universitat de València, where he is currently an Associate Professor and a member of the Laboratory of Industrial Electronics and Instrumentation (LEII).

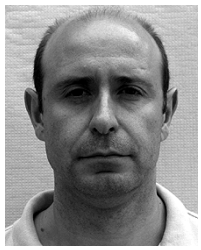

Agustin Ferreres was born in Sant Mateu, Spain, in 1963. He received the M.Sc. degree in physics, with a specialization in electronics, and the Ph.D. degree from the Universitat de València, Burjassot, Spain, in 1993 and 1999, respectively.

He was with GH Electrotermia S.A. for two years. In 1995, he joined the Laboratory of Industrial Electronics and Instrumentation (LEII) at the Universitat de València, where he is currently an Associate Professor. His main research areas include industrial electronics, power supplies, and space power systems.

Enrique J. Dede (M'89) received the Ph.D. degree in electronics from the Universitat de València, Burjassot, Spain.

He is a Full Professor of Power Electronics at the Universitat de València, Director of the Laboratory of Industrial Electronics and Instrumentation (LEII), and R&D Director of the company GH Electrotermia S.A. He has more than 20 years of experience in the design of high-frequency inverters and has authored more than 250 papers in the area of power electronics. He is the holder of several international patents on high-frequency inverters for induction heating.

Dr. Dede is a Member of the European Working Group of the IEEE Industry Applications Society, of the International Advisory Board of PCIM Europe, and of the Steering Committee of EPE. He is the President of the Spanish Chapter of the IEEE-PELS Society.

Vicente Esteve (M'03) was born in Valencia, Spain, in 1961. He received the M.Sc. and Ph.D. degrees from the Universitat de València, Burjassot, Spain, in 1986 and 1999, respectively.

He is currently an Associate Professor at the Universitat de València. His research activities include high-frequency rectifiers and inverters and electronic instrumentation. He has more than 17 years of experience in the design and test of power electronic equipment.

José Jordán was born in València, Spain, in 1964. He received the M.Sc. and Ph.D. degrees from the Universitat de València, Burjassot, Spain, in 1989 and 2003, respectively.

He is currently an Assistant Professor at the Universitat de València. His main research activities include high-power inverters for induction heating and components characterization. He is a Consultant to G.H. Electrotermia S.A. in the field of induction tube welding and advanced topologies. He has more than 14 years experience in the design of high-frequency inverters for induction tube welding and high-power-output transformers.

Rafael García-Gil was born in Granja-Costera, Spain, in 1970. He received the M.Sc. degree in physics and the M.Sc. and Ph.D. degrees in electronics engineering from the Universitat de València, Burjassot, Spain, in 1993, 1995, and 2002, respectively.

He is currently an Assistant Professor at the Universitat de València. His main research areas are four-quadrant converters with power-factor correction and magnetic components modeling.